JACS
JOURNAL OF THE AMERICAN CHEMICAL SOCIETY

Article

pubs.acs.org/JACS

Peripherally Fused Porphyrins via the Scholl Reaction: Synthesis, Self-Assembly, and Mesomorphism

Damian Myśliwiec,[†] Bertrand Donnio,[‡] Piotr J. Chmielewski,[†] Benoît Heinrich,[‡] and Marcin Stępień*[,†]

[†]Wydział Chemii, Uniwersytet Wrocławski, ul. F. Joliot-Curie 14, 50-383 Wrocław, Poland

[‡]Institut de Physique et Chimie des Matériaux de Strasbourg, CNRS-Université de Strasbourg (UMR7504), BP 43, F-67034 Strasbourg Cedex 2, France

Supporting Information

ABSTRACT: Oxidative coupling of activated aryl groups attached to β-positions of the porphyrin ring provides convenient access to derivatives containing peripherally fused phenanthrene and benzo[*g*]chrysene units. Tetra(benzochryseno)porphyrin, reported here for the first time, contains a nonplanar, sterically locked π system and shows very intense electronic absorptions in the Q range of the electronic spectrum. Tetraphenanthroporphyrins show a tendency to aggregate in solution. In one case, a discrete dimer is formed, whose structure was investigated spectroscopically and theoretically. Derivatives bearing long alkyl chains are mesomorphic and exhibit columnar phases (tetraphenanthroporphyrins) and a monoclinic 3D phase (tetrabenzochrysenoporphyrin). The symmetry of column packing in the columnar phases is dependent on the number of alkyl chains per molecule. X-ray diffraction measurements show that, in spite of their nonplanarity, the aromatic cores in the mesophases are tightly stacked within the column. The corresponding stacking patterns were derived from the structure of the dimer, on the basis of geometrical analysis and molecular modeling.

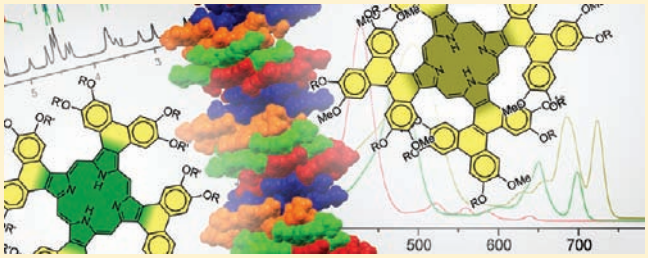

INTRODUCTION

Organic structures with extensive, two-dimensional (2D) π-conjugation play an increasingly important role in materials chemistry.[1] Several classes of motifs, such as hexa-*peri*-benzocoronenes,[1a] porphyrins,[1b,c] and phthalocyanines,[1c,d] have been investigated as electroactive cores for organic semiconductors and photovoltaic devices.[2] On the molecular level, properties of these materials, such as charge carrier mobilities,[2b,d] n- vs p-type semiconductivity,[2c] etc., can be tailored in two ways: by designing new core motifs and by controlling the self-assembly of the molecules in the bulk. A high level of structural control is frequently achieved through self-organization into well-defined, usually columnar mesophases,[3] which facilitate fabrication of large-area thin devices and are solution processable.[2a]

The electronic properties of core motifs strongly depend on the extent of π-conjugation, and increasing the size of the π system is advantageous in many potential applications. A number of useful methods of "supersizing" the π-electron system have evolved in the context of porphyrinoid chemistry. The most successful strategies include macrocycle expansion,[4] construction of multiporphyrin arrays,[5] and fusion of additional rings on the periphery of the macrocycle.[6−8] To date, peripherally fused macrocycles have been made by condensation of fused monopyrroles (Scheme 1, route A),[6,8e−k] by aromatization of peripheral rings in a preformed macrocycle (route B),[8a−d] or by oxidative fusion of meso substituents (route C).[5a−e,7] A complementary strategy can be envisaged, in which the expansion of the porphyrin π-electron system is achieved by fusing adjacent β substituents (route D). In spite of its apparent simplicity, this route remains largely unexplored.[9] Here we show that appropriately designed β-aryl porphyrins afford peripherally fused derivatives when subjected to Scholl-type oxidations. This strategy provides access to large, fused aromatic cores, which display promising chromophore properties and are easily functionalized on the periphery. Peripheral functionalization of these macrocycles provides a means of controlling their π-stacking self-assembly both in solution and the liquid-crystalline state.[10]

RESULTS AND DISCUSSION

Synthesis and Characterization of Tetraphenanthroporphyrins. We focused our initial synthetic efforts on 2,3,7,8,12,13,17,18-octakis(3,4-dialkoxyphenyl)porphyrins **2a**−**c**-H_2, containing, respectively, none, 8, and 16 dodecyloxy chains per molecule (Scheme 2). The alkoxy groups were introduced as convenient functionalization sites and as a means of activating the aryl substituents toward oxidative coupling reactions. Porphyrins **2a**−**c**-H_2 were prepared by condensing appropriate monopyrroles **1a**−**c**,[11] which in turn were synthesized via a modified Zard−Barton reaction[12] (see

Received: November 22, 2011
Revised: December 18, 2011
Accepted: January 9, 2012
Published: January 9, 2012

   dx.doi.org/10.1021/ja210991f | *J. Am. Chem. Soc.* 2012, 134, 4822−4833

Scheme 1. Synthetic Routes to Peripherally Fused Porphyrins[a]

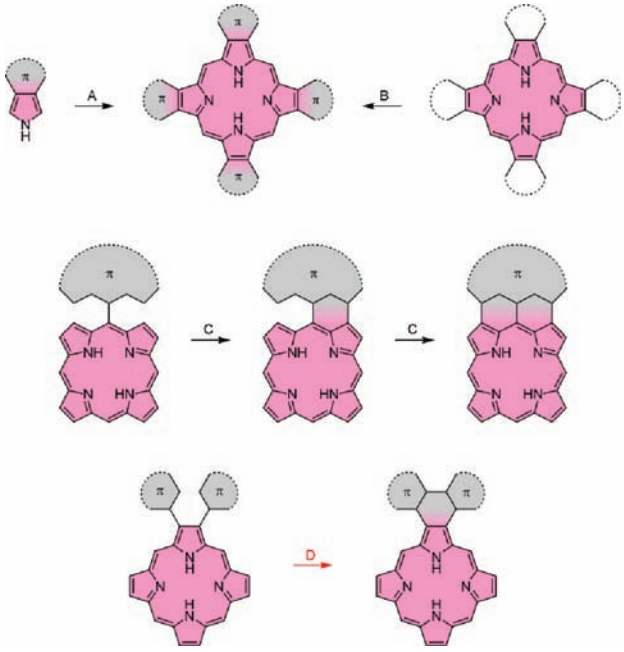

[a] "π" denotes a π-conjugated ring or ring system. (A) From fused monopyrroles. (B) Aromatization of peripheral rings. (C) Fusion of meso-substituents. (D) Fusion of β substituents (this work)

Supporting Information). Scholl oxidations were performed on zinc complexes **2b**-Zn and **2c**-Zn using 12 equiv of anhydrous ferric chloride in dichloromethane, yielding alkoxy-substituted tetraphenanthroporphyrins **3b**-H_2 and **3c**-H_2 in 74% and 97% isolated yield, respectively.

The starting zinc complexes **2b**-Zn and **2c**-Zn are demetalated in the course of the oxidation, most likely because of the acidic reaction conditions. Even though the oxidation can be performed on the free bases **2b**-H_2 and **2c**-H_2, the use of zinc complexes offers higher yields and shorter reaction times. In contrast, because of the very low solubility of **2a**-Zn, the all-methoxy derivative **3a**-H_2 was more conveniently prepared by reacting the free base **2a**-H_2 with $FeCl_3$ in *o*-dichlorobenzene. The free bases **3a**−**c**-H_2 are easily metalated to the corresponding Zn complexes under standard conditions.

Scholl-type oxidative couplings are known to proceed cleanly for many types of aromatic rings.[1a] In some cases though, the yields of these reactions are compromised by low regioselectivity and unwanted side reactions (competition between inter- and intramolecular coupling, oligomerization, quinone formation, etc.)[13] In the present work, the 3,4-dialkoxyphenyl substituents in **2a**−**c**-H_2 are activated toward oxidative coupling at both ortho positions (2 and 6), and mixtures of products corresponding to both 2−2′ and 2−6′ coupling (Scheme 2) could potentially be observed. In the reactions described above, tetraphenanthroporphyrins are obtained as pure regioisomers, suggesting that the 2−6′ coupling route is strongly disfavored.

Scheme 2. Synthesis of Tetraphenanthro- and Tetra(benzochryseno)porphyrins Using the Scholl Reaction[a]

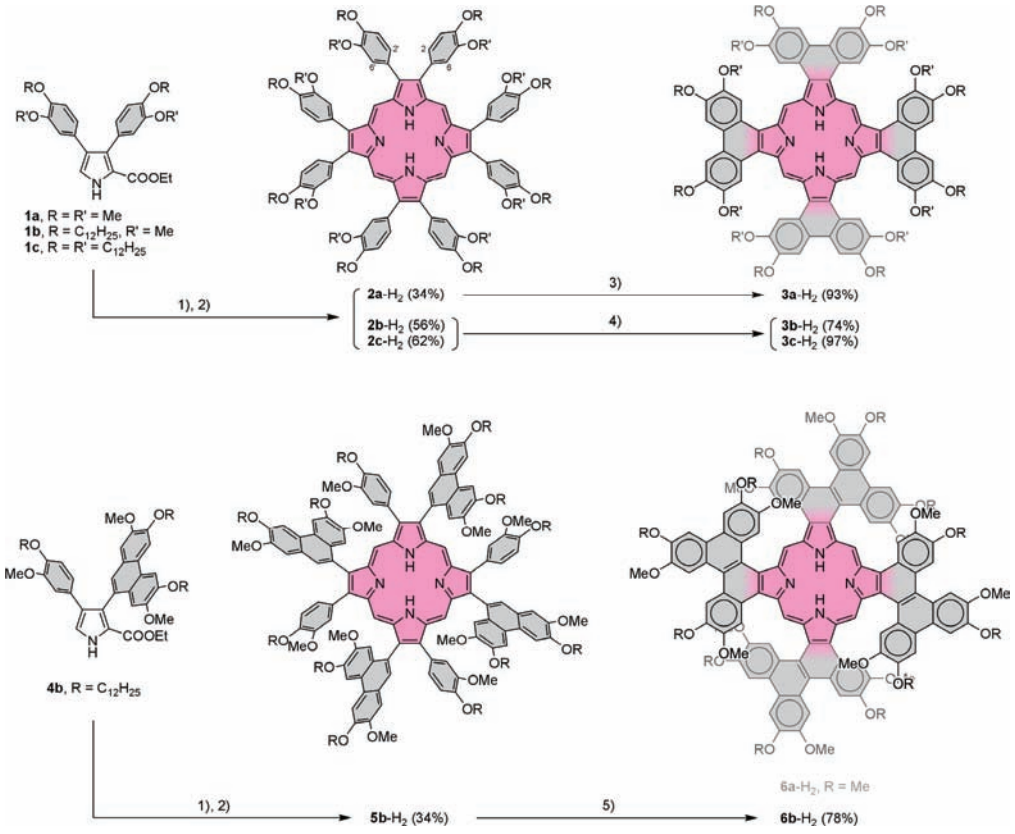

[a]Reagents and conditions: (1) $LiAlH_4$, THF; (2) $CHCl_3$, $BF_3{\cdot}Et_2O$, then DDQ or chloranil; (3) $FeCl_3$, *o*-dichlorobenzene; (4) (a) $Zn(OAc)_2$, $CHCl_3$/MeOH; (b) $FeCl_3$, CH_2Cl_2; and (5) $BF_3{\cdot}Et_2O$, DDQ, CH_2Cl_2

dx.doi.org/10.1021/ja210991f | J. Am. Chem. Soc. 2012, 134, 4822−4833

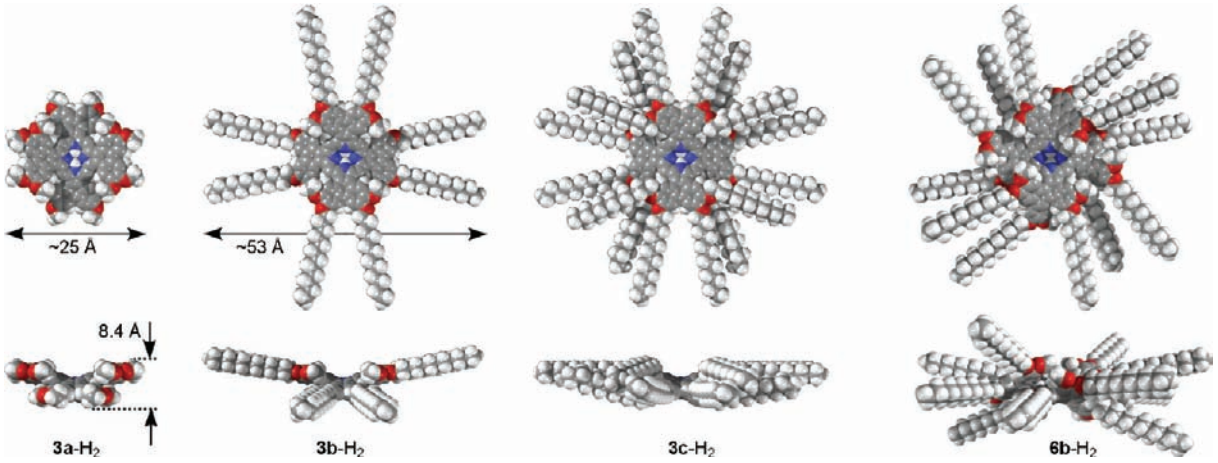

Figure 1. van der Waals models of **3a**−**c**-H_2 and **6b**-H_2 based on DFT optimized geometries (B3LYP/6-31G**).

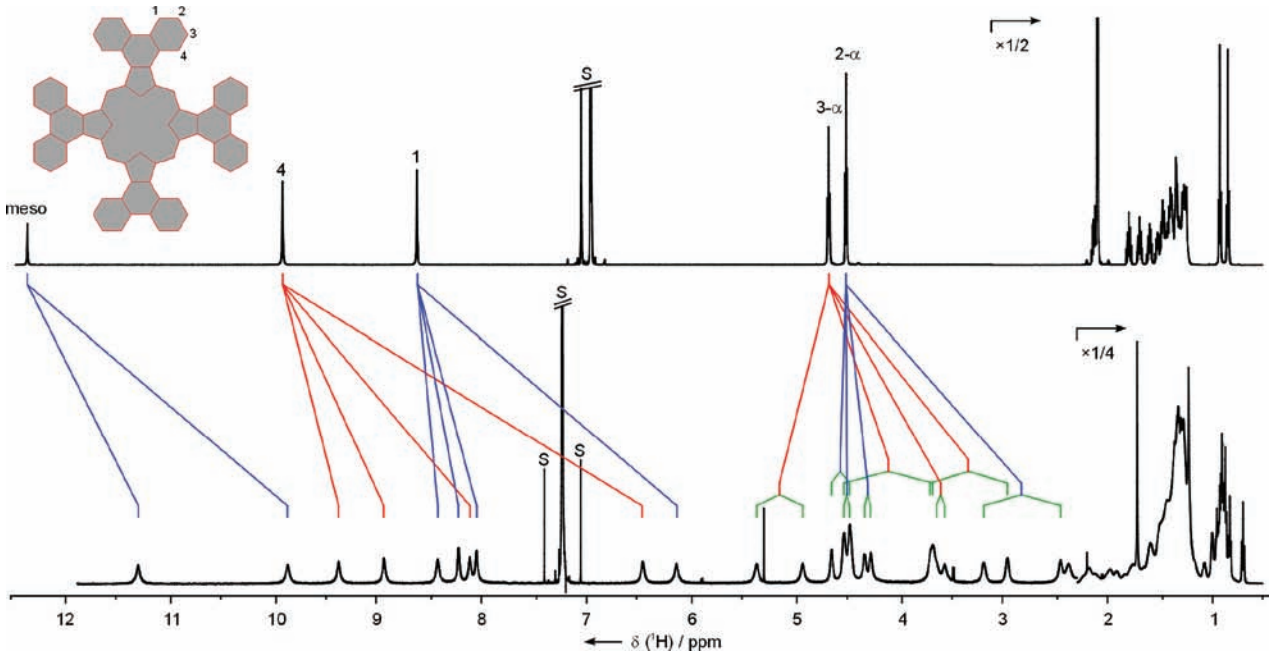

Figure 2. ^{1}H NMR spectrum of **3c**-Zn (top, 600 MHz, toluene-d_8, 380 K) and its dimer (**3c**-Zn)$_2$ (bottom, 600 MHz, chloroform-*d*, 230 K). Blue and red lines correlate signals of the monomer with those of the dimer. Green lines connect diastereotopic pairs of α-CH_2 signals. The numbering scheme is shown in the inset.

The identity of phenanthroporphyrins and their complexes was confirmed by ^{1}H and ^{13}C NMR spectroscopy, high-resolution mass spectrometry, and electronic absorption spectroscopy. Proton magnetic resonance spectra of **3a**−**c**-H_2 and **3a**−**c**-Zn show signal patterns consistent with the formation of phenanthrene moieties. Specifically, the low-field region of the spectrum contains three singlets, corresponding to the meso protons and the two sets of protons attached to phenanthrene units. The significant downfield shift of the meso signal (~11.9 ppm) is likely caused by the deshielding effect of the flanking phenanthrenes.

Three-dimensional structures of the free base tetraphenanthroporphyrins **3a**−**c**-H_2 were modeled using density functional theory (B3LYP/6-31G**, Figure 1). Initially, it was recognized that the macrocyclic core of **3a**-H_2 cannot be planar because of steric interactions between the neighboring phenanthrene units. Consequently, geometries of the four distinct conformers of **3a**-H_2 were optimized (Supporting Information). Remarkably, relative energies of the four conformers span a range of only 2 kcal/mol. The conformer with lowest energy, shown in Figure 1, has a saddle-type distortion corresponding to the effective D_{2d} symmetry in the limit of fast tautomerization. This structure qualitatively resembles geometries predicted for meso-substituted derivatives,[8i] except that the degree of out-of-plane deformation is much smaller. The molecule of **3a**-H_2 is roughly disk-shaped with the van der Waals diameter of ca. 25 Å. This value increases to ca. 53 Å for **3b**-H_2 and **3c**-H_2, both of which were modeled with fully outstretched dodecyl chains. The nonplanarity of **3b**−**c**-H_2 is not observed in the experimental ^{1}H NMR spectra recorded at room temperature, which correspond to effective D_{4h} symmetry. Any nonplanar structure should exhibit diastereotopic differentiation of α-CH_2 groups. The absence of this feature indicates that nonplanarity in tetraphenanthroporphyrins is averaged out by conformational motions in solution.

dx.doi.org/10.1021/ja210991f | J. Am. Chem. Soc. 2012, 134, 4822−4833

At room temperature, ^{1}H NMR spectra of alkoxy-substituted phenanthroporphyrins and their complexes show a varying degree of line broadening, which is dependent on sample concentration, temperature, and solvent. This effect is attributable to π-stacking aggregation in solution,[14] which is likely promoted by the extended π-surface of the macrocycle. Indeed, no similar line broadening is observed for the unoxidized species **2a**−**c**-H_2 and **2a**−**c**-Zn, in which the β-aryl substituents are not coplanar with the macrocycle, thus likely suppressing aggregation. The line broadening effect becomes very strong for the zinc(II) complexes **3b**-Zn and **3c**-Zn. A well-resolved ^{1}H NMR spectrum of the latter species was nevertheless recorded in toluene-d_8 at 380 K (Figure 2). In the case of **3c**-Zn, π-stacking interactions lead to the equilibrium formation of a well-defined aggregate, as can be inferred from the ^{1}H NMR spectra recorded in chloroform-d over a range of temperatures. At 300 K, the spectrum contains broadened signals corresponding to the fully symmetric monomer and to a species of lower symmetry, which yields exchange correlations with the monomer signals in the NOESY spectrum. As the temperature is lowered, the molar fraction of the low-symmetry species increases, and at 230 K, the monomer is no longer observed (Figure 2). In dichloromethane-d_2, the low-symmetry species prevails, and signals of the monomer are not observed even at 290 K. In the latter solvent, lowering the temperature below 260 K causes dramatic broadening of all signals, and no decoalescence is observed down to 190 K.

Even though the low-symmetry spectra observed in chlorinated solvents are quite broad at all accessible temperatures, partial assignment of signals was obtained from the analysis of correlation spectra, providing evidence consistent with the formation of a dimer, [**3c**-Zn]$_2$. The effective symmetry of a single macrocyclic subunit in the proposed dimer structure is reduced from D_{4h} to C_s, with the plane of symmetry passing through two opposite phenanthrene moieties. Consequently, the ^{1}H NMR spectrum of [**3c**-Zn]$_2$ contains two meso signals, eight phenanthrene signals (denoted 1 and 4 in Figure 2), and eight diastereotopic pairs of α-CH_2 signals. On the basis of the observed spectral symmetry, it can be assumed that the two macrocyclic subunits are not stacked directly one above the other but displaced laterally. In such a structure, the diastereotopic differentiation of α-methylene signals is consistent with the two faces of the macrocycle being nonequivalent. The signals of the meso and phenanthrene protons in [**3c**-Zn]$_2$ show consistent upfield relocations (up to ca. 3 ppm) relative to their positions in the monomer. Such an effect is expected for two stacked aromatic rings, which experience mutual shielding caused by their respective ring currents.[14c]

The [**3c**-Zn]$_2$ dimer can be considered a structural prototype for larger π-stacked assemblies of tetraphenanthroporphyrins, including those involved in the formation of discotic mesophases (see below). Unfortunately, systematic theoretical exploration of the dimerization process is a complex task, given the size of the system, the number of degrees of freedom, and the necessary level of theory. For an initial qualitative analysis, the problem can be simplified by considering structures containing only methoxy groups, namely [**3a**-H_2]$_2$ and [**3a**-Zn]$_2$. These structures were modeled using a high-level dispersion-corrected DFT method (ωB97XD/6-31G**) and, for comparison, with a general-utility molecular mechanics force field (MM+, Hyperchem).[15]

Initial screening of several structures showed that the interaction energy in the dimer strongly depends on the extent of overlap between the two π systems. High stabilization was observed for dimers consisting of two saddle-shaped ($\sim D_{2d}$) conformers combined into a laterally displaced sandwich (Figure 3). Two modes of interaction, C_{2h} and C_2, could be

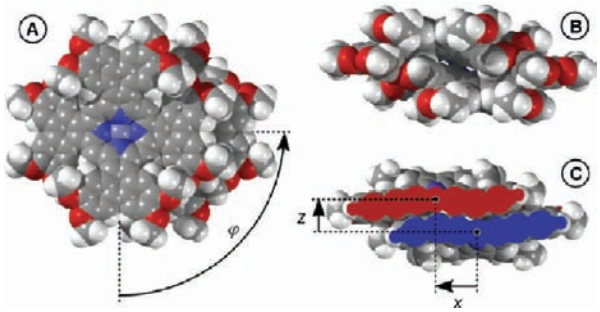

Figure 3. Optimized structure of [**3a**-Zn]$_2$ (ωB97XD/6-31G**). (A) Top and (B) side views and (C) side view cross section revealing the stacking interaction between the cores. Red and blue colors denote the two interacting components of the dimer. For definitions of z, x, and φ, see footnote of Table 1.

distinguished for [**3a**-H_2]$_2$. Each of these modes provides a large contact area between the two π surfaces but differs in the in-plane alignment of the two molecules. Locally, the separation between monomer molecules in the DFT and MM models can be as small as 3.3 Å, which is a typical π−π stacking distance. The two curved π-systems are oriented in such a way that the convex side of a phenanthrene unit in one molecule is placed above the saddle-shaped center the other molecule. The C_{2h} structure of [**3a**-H_2]$_2$ is consistent with the symmetry of the ^{1}H NMR spectrum of [**3c**-Zn]$_2$ and is predicted to be more stable than [**3a**-H_2]$_2$-C_2 by ca. 8.7 kcal/mol (Table 1). The energy gap between C_{2h} and C_2 structures is relatively small when compared with the dimerization energies.

Table 1. Calculated Energies and Geometrical Parameters of Dimers [3a-H_2]$_2$ and [3a-Zn]$_2$

species	method	E [kcal/mol][a]	z [Å][b]	x [Å]	φ [°]
[**3a**-H_2]$_2$-C_{2h}	DFT[c]	76.23	3.97	5.49	90
	MM[d]		3.86	4.49	90
[**3a**-H_2]$_2$-C_2	DFT	67.55	4.11	5.68	107
	MM		4.14	5.44	105
[**3a**-Zn]$_2$-C_{2h}	DFT	83.89	3.57	4.40	90

[a]Dimerization energies relative to optimized monomers (gas phase, counterpoise-corrected DFT energies). [b]z is the stacking distance calculated as the distance between the N_4 centroid of one molecule and the N_4 mean plane of the other molecule; x is lateral offset, calculated as $x = (r^2 - z^2)^{1/2}$, where r is the distance between the two N_4 centroids; φ is the approximate angle necessary to superimpose the molecules after translating one of them onto the other along the z and x vectors. [c]ωB97XD/6-31G**. [d]MM+ force field (Hyperchem).

For the sake of subsequent discussion of mesophase structures, it is convenient to quantify the interaction geometry in the dimers using three parameters: the separation of mean N_4 planes of the two macrocycles (z), the lateral offset of ring centers (x), and the rotation angle φ (Table 1, Figure 3). The overlap of the two π systems is larger in the Zn complex as evidenced by the smaller value of the lateral offset x. In line

dx.doi.org/10.1021/ja210991f | J. Am. Chem. Soc. 2012, 134, 4822−4833

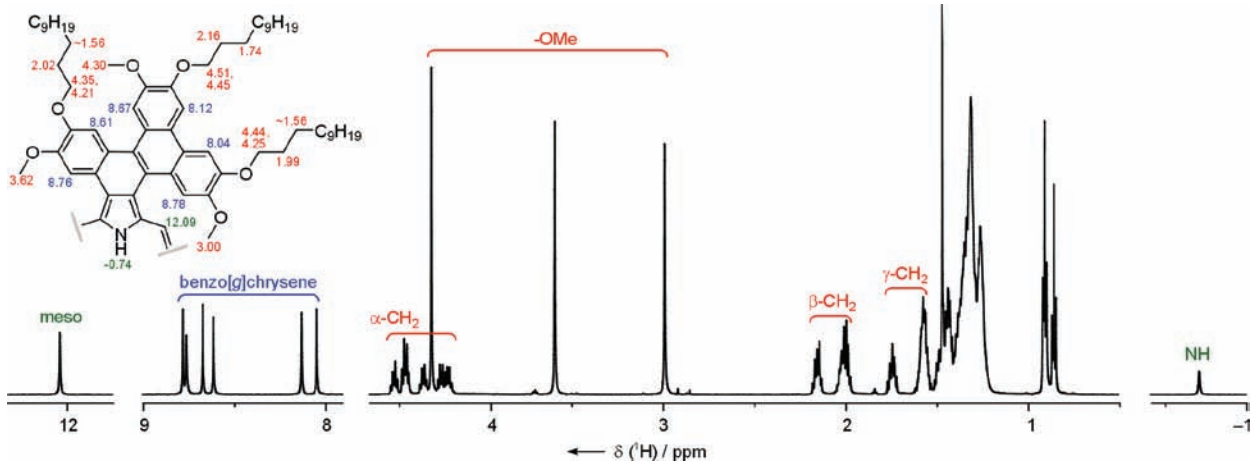

Figure 4. ^{1}H NMR spectrum of tetra(benzochryseno)porphyrin 6b-H_2 (600 MHz, chloroform-*d*, 325 K). The assignment of signals was obtained from correlation spectroscopy. For additional NMR data, see Supporting Information.

with this observation, the gas-phase interaction energies calculated by DFT are 83.89 and 76.23 kcal/mol for [**3a**-Zn]$_2$-C_{2h} and [**3a**-H_2]$_2$-C_{2h}, respectively. These values are significantly larger than the dimerization energies calculated for dimers of porphine,[15c] reflecting the expansion of the aromatic core in tetraphenanthroporphyrins and, possibly, the presence of alkoxy substituents, which can be involved in additional stabilizing nonbonded interactions. Interestingly, the geometries of [**3a**-H_2]$_2$-C_{2h} and [**3a**-H_2]$_2$-C_2 optimized using the MM+ force field are in fairly good agreement with the DFT structures.

Tetra(benzochryseno)porphyrin. The oxidative coupling strategy described above for octaarylporphyrins is also applicable to porphyrins bearing polycyclic aromatic substituents, such as **5b**-H_2 (Scheme 2). This porphyrin, which bears four phenyl and four 9-phenanthryl groups, was obtained from the corresponding monopyrrole **4b** in 34% yield. The condensation step proceeds without observable scrambling (reversible dissociation of oligopyrrole intermediates[16]), yielding just one regioisomer. However, **5b**-H_2 is isolated as a mixture of atropisomers resulting from the restricted rotation of the bulky phenanthryl substituents.[14c] In an initial synthetic attempt, this isomeric mixture was converted into the zinc(II) complex **5b**-Zn, which was in turn subjected to oxidative coupling with $FeCl_3$. After workup, tetra(benzochryseno)-porphyrin[17] **6b**-H_2 was isolated in 42% yield. A more efficient synthesis was therefore sought: It was found that the free base **5b**-H_2 would produce the desired benzochryseno- derivative in yields of up to 78% when treated with four equivalents of DDQ in the presence of boron trifluoride etherate. **6b**-H_2 is easily metalated to provide the zinc complex **6b**-Zn.

The ^{1}H NMR spectrum of **6b**-H_2 is consistent with the presence of 4-fold symmetry in the molecule, providing additional indication that the parent porphyrin **5b**-H_2 used for oxidation was a pure etio I-type isomer (Figure 4). The alkoxy-substituted benzo[*g*]chrysene system fused to each pyrrole ring gives rise to six singlets in the aromatic region, which are accompanied by signals corresponding to three nonequivalent methoxy groups and three dodecyloxy chains. The α-methylene groups within the chains exhibit marked diastereotopicity, indicating that the macrocycle is not planar and the nonplanarity is not averaged out by conformational motions in solution. Apparently, in contrast to tetraphenanthroporphyrins, **6b**-H_2 is sterically "locked" because the benzochrysene subunits eclipse each other to a greater extent than phenanthrene rings in compounds **3a**−**c**-H_2. This eclipsing arrangement of aromatic rings in **6b**-H_2 causes substantial shielding of one of the methoxy groups, which resonates at 3.00 ppm.

To gain further insight into the three-dimensional structure of tetra(benzochryseno)porphyrins, a number of conformers of the all-methoxy variant, **6a**-H_2 (not synthesized) were optimized at the B3LYP/6-31G** level of theory. The lowest energy conformer was found to have the expected alternating arrangement of fused subunits similar to that found in tetraphenanthroporphyrins. Each of the subunits is internally twisted so as to reduce congestion in the fjord regions,[18] resulting in a highly nonplanar but rather tightly packed aromatic structure. The preferred conformation has the S_4 point symmetry (in the limit of fast tautomerization), in line with the observed NMR spectral pattern. Reoptimizing the structure with dodecyl chains attached provides a plausible 3D model of **6b**-H_2 (Figure 1). As a consequence of the out-of-plane distortion, the aromatic core of **6b**-H_2 is significantly thicker than the cores of tetraphenanthroporphyrins. However, the diameter of the molecule (55.5 Å, including the dodecyl chains) is only slightly larger than those of **3b**−**c**-H_2 in spite of the additional fused benzene rings.

Electronic Structure. Expansion of the π-conjugated system by peripheral ring fusion strongly affects the electronic absorption profiles of tetraphenanthro- and tetra(benzochryseno)porphyrins and their zinc(II) complexes (Figure 5). With the increasing size of the π system, both Soret and Q bands are shifted bathochromically relative to their positions in the spectra of parent porphyrins (Table 2). The spectra of tetraphenanthroporphyrins, which show no significant dependence on the alkyl substitution pattern, are qualitatively similar to those reported earlier for differently substituted species.[8e] In particular, λ_{max} increases by ca. 60 nm on going from porphyrin **2c**-H_2 to tetraphenanthroporphyrin **3c**-H_2, which contains 12 fused benzenoid rings). Interestingly, further extension of the π system in **6b**-H_2, which involves fusion of eight additional rings, leads to a smaller bathochromic shift of 25 nm relative to **3c**-H_2. This observation shows that when peripheral ring fusion occurs at a distance from the porphyrinic core, it becomes less efficient at decreasing the

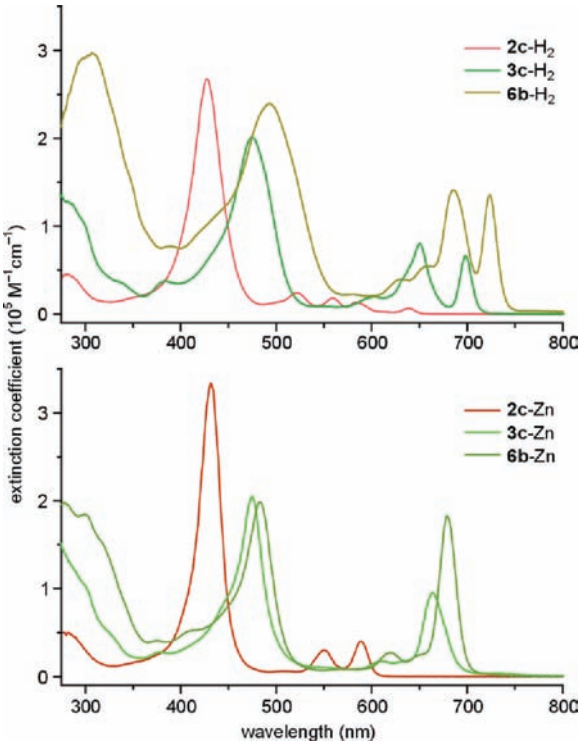

Figure 5. Electronic spectra of porphyrin **2c**-H_2, tetraphenanthroporphyrin **3c**-H_2, tetra(benzochryseno)porphyrin **6b**-H_2, and their zinc(II) complexes (dichloromethane, 293 K).

Table 2. Electronic Properties of Porphyrins and Their Analogues Discussed in the Text

	absorptions [nm]		HOMO–LUMO gap [eV, V]		
species	Soret	λ_{max}	UV–vis[a]	CV[b]	DFT[c]
2c-H_2	427	639	1.94	2.27	2.10
3c-H_2	474	698	1.78	1.66	1.92
6b-H_2	493	724	1.71	1.77	1.82
2c-Zn	431	589	2.11	2.18	2.22
3c-Zn	475	664	1.87	1.76	1.96
6b-Zn	483	679	1.83	1.75	1.86

[a]Calculated from λ_{max} [eV]. [b]$E_{ox} - E_{red}$, measured by cyclic voltammetry [V]. [c]B3LYP/6-311G**//B3LYP/6-31G** [eV]; calculated for all-methoxy-substituted structures (**2a**-H_2, **3a**-H_2, etc.). For complete UV–vis, electrochemistry, and DFT data, see the Supporting Information.

highest occupied–lowest unoccupied molecular orbital (HOMO–LUMO) gap. This conclusion is confirmed by electrochemistry data and DFT calculations (Table 2). Cyclic voltammetry measurements reveal that expansion of the π system in the sequence **2c**-M, **3c**-M, **6b**-M (M = 2H or Zn) results in gradual anodic shifting of the first reduction potential. Interestingly, the change is not systematic in the case of the first oxidation potential, which decreases in the sequence **2c**-M > **6b**-M > **3c**-M. As a consequence, the electrochemically determined HOMO–LUMO gaps for tetra(benzochryseno)porphyrins are comparable to or slightly larger than those of their tetraphenanthro- couterparts. The calculated HOMO–LUMO gaps are overestimated by ca. 0.1 eV, which is an expected deviation at the employed level of theory,[19] but the decrease of the gap with increasing conjugation is well reproduced.

While the red shifts observed in **3a–c**-H_2 and **6b**-H_2 are much smaller than those reported for the best meso-arene-fused porphyrins,[7f] the expansion of the π system leads to a substantial increase in the intensity of Q bands.[20] The maximum Q-band intensity increases from 24 100 (**2c**-H_2, 522 nm), through 80 300 (**3c**-H_2, 650 nm), up to 141 000 $M^{-1}cm^{-1}$ (**6b**-H_2, 686 nm). The latter value compares favorably with those reported for Q bands of cyclo[8]-pyrroles[21,10c] ($\sim 1.3 \times 10^5$ $M^{-1}cm^{-1}$) and a quadruply anthracene-fused porphyrin[7f] ($\sim 1.2 \times 10^5$ $M^{-1}cm^{-1}$). A similar trend is observed for zinc complexes, with the principal Q-band in **6b**-Zn reaching ε = 183 000 $M^{-1}cm^{-1}$

Kohn–Sham orbitals obtained from DFT calculations for the all-methoxy-substutited structures **3a**-H_2 and **6a**-H_2 are shown in Figure 6. In each case, the range of orbitals included covers those principally involved in the strongest electronic transitions, as predicted by TD-DFT. In the case of tetraphenanthroporphyrin **3a**-H_2, the two lowest-lying excited states, assumed to represent experimental Q bands, are mixtures of excitations involving the four orbital range (364–367, Figure 6), corresponding to the Gouterman model.[22] For higher-energy states, including those responsible for the Soret absorption, the range of occupied levels involved is larger, leading to considerable mixing of excitations. In the case of tetra(benzochryseno)porphyrin **6a**-H_2, the most intense Q-band excited states are mixtures of excitations from levels 533, 532, and 528. It is noteworthy that the MO coefficients on the extra benzene rings fused to **6a**-H_2 are rather small in the frontier orbitals (especially in LUMO and LUMO+1). This might explain the small bathochromic shift in tetra(benzochryseno)-porphyrin relative to tetraphenanthroporphyrin.

Mesomorphism. The thermal phase behavior of porphyrins **2b–c**-M, tetraphenanthroporphyrins **3b–c**-M (M = 2H, Zn) and zinc tetra(benzochryseno)porphyrin **6b**-Zn was investigated using small-angle X-ray diffraction (XRD, Table 3), differential scanning calorimetry (DSC, Figure 7), and polarizing optical microscopy (POM).[23] With the exception of **3b**-H_2,[24] all of the materials analyzed form well-defined liquid crystalline phases, often exhibiting broad ranges of thermal stability. Three distinct types of 2D and 3D phases were identified, whose structural diversity results from variations of the substitution pattern and the nature of the core motif.

Compounds **2b**-H_2 and **2b**-Zn, both containing eight dodecyl chains per molecule, exhibit structurally similar Col_h phases. The hexagonal symmetry of these phases was assigned unequivocally on the basis of the XRD patterns, containing one or two sharp reflections in the small-angle region. Close inspection of the wide-angle scattering revealed the presence of three overlapping signals: (i) a large diffuse halo associated with molten aliphatic chains (h_{ch}, correlation length ξ = 10 Å), showing the largest temperature shift,[25] (ii) the typical h_0 signal at 3.6 Å, resulting from π–π stacking of aromatic rings, and (iii) an additional semidiffuse reflection at ca. 4.7 Å ($\xi \approx 50$ Å), denoted h_{por}. The occurrence of these three diffuse wide-angle signals strongly suggests a double-segregation process, leading to one-dimensional stacking of porphyrins into columns, with the peripheral aromatic systems segregated from both the aliphatic continuum and the central porphyrin cores. The h_{por} signal, clearly identifiable for **2b**-H_2 and **2b**-Zn, is in good agreement with interplanar distances between stacked macrocyclic rings, observed in the solid-state structures of β-aryl-substituted porphyrins.[26] Furthermore, the average molecular thickness h_M of **2b**-H_2 and **2b**-Zn, calculated as the ratio of

dx.doi.org/10.1021/ja210991f | J. Am. Chem. Soc. 2012, 134, 4822–4833

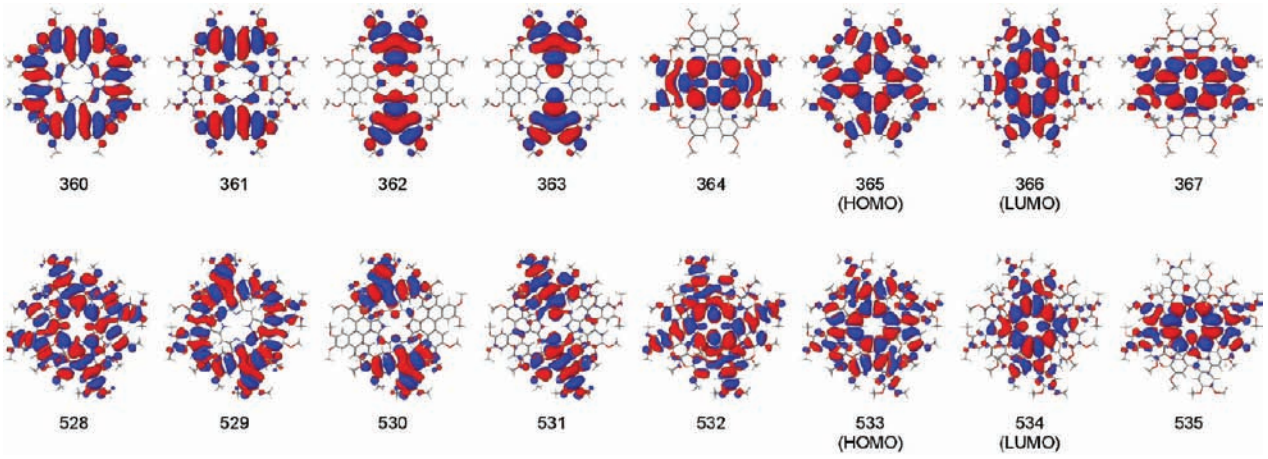

Figure 6. Highest occupied and lowest unoccupied Kohn–Sham orbitals of tetraphenanthroporphyrin (**3a**-H_2, top) and tetra(benzochryseno)-porphyrin (**6a**-H_2, bottom) calculated at the B3LYP/6-311G**//B3LYP/6-31G** level of theory (cutoff level 0.009 au).

Table 3. Geometrical Parameters of Mesophases Obtained from XRD

		lattice parameters[a,b]					core parameters[a]								
species	T [°C]	type	$a \times b \times c$ [Å]	q_{hex}[c]	h_M[d] [Å]	V_M[e] [10^3 Å^3]	V_c[f] [10^3 Å^3]	S_c[g] [Å^2]	σ_c[h] [Å^2]	ψ_c[i] [°]	D_c[j] [Å]	d_c[j] [Å]	d_c/D_c[j]	Σ_c[k] [Å^2]	q_{ch}[l]
2b-H_2	235	Col_h	34.5	1	5.3	5.45	2.19	4.16	416	0	23.0		1	381	0.97
2b-Zn	190	Col_h	34.8	1	5.1	5.32	2.16	4.24	424	0	23.2		1	372	0.97
3b-Zn	140	Col_h	34.5	1	5.0	5.16	2.11	4.21	421	0	23.2		1	364	0.98
2c-H_2	120	Col_{r1}	53.1 × 36.6	0.84	7.9	7.67	2.11	2.67	424	51.0	23.2	14.6	0.63	476	1.30
	160	Col_{r2}	63.4 × 30.0	1.22	8.3	7.86	2.14	2.59	424	52.4	23.2	14.2	0.61	492	1.31
2c-Zn	100	Col_{r1}	52.6 × 36.6	0.83	7.9	7.58	2.09	2.66	424	51.2	23.2	14.6	0.63	473	1.31
3c-H_2	120	Col_{r1}	52.5 × 37.2	0.82	7.9	7.66	2.09	2.67	421	50.7	23.2	14.7	0.63	472	1.29
3c-Zn	100	Col_{r1}	56.0 × 38.1	0.85	7.1	7.57	2.08	2.93	421	45.9	23.2	16.1	0.70	441	1.22
6b-Zn	150	Mon	68.2 × 39.0 × 81.0[m]	1.01	5.7	7.69	3.07	5.36	*614*[n]	*29.0*	28.0	*24.4*	–	*472*	*0.84*

[a]See Figure 8 for definitions of relevant parameters and Table S6, Supporting Information for complete data and formulas used. [b]Lattice symmetries are *p6mm* (2D, Col_h), *c2mm* (2D, Col_{r1} and Col_{r2}), and $P2_1/m$ (3D, Mon). [c]Sublattice compression ratio relative to an ideal hexagonal lattice; $q_{hex} = a'/(b'\sqrt{3})$ and for Col_r phases $a' = a$, $b' = b$ and for the Mon phase $b' = b$, $a' = d_{001}$. [d]Columnar slice thickness. [e]Molecular volume at the given temperature. [f]Partial volume of the molecular core (alkyl chains and methyl groups excluded from the calculation). [g]Effective cross-section of the core perpendicular to the column axis, $S_c = V_c/h_M$. [h]Cross-section of the core in the absence of tilt. $S_c = \sigma_c$ for nontilted phases. [i]Tilt angle of cores relative to column axis. [j]Maximum (D_c) and minimum (d_c) diameters of the elliptical cross-section S_c; d_c/D_c ratio is the ellipticity of the core. [k]Interface area between the core and the aliphatic periphery. [l]Chain packing ratio; for explanation see text. [m]$\beta = 98.0°$, and $V = 2.13 \times 10^5$ Å^3. [n]Parameters in italics are calculated for hypothetical tilted packing of column segments.

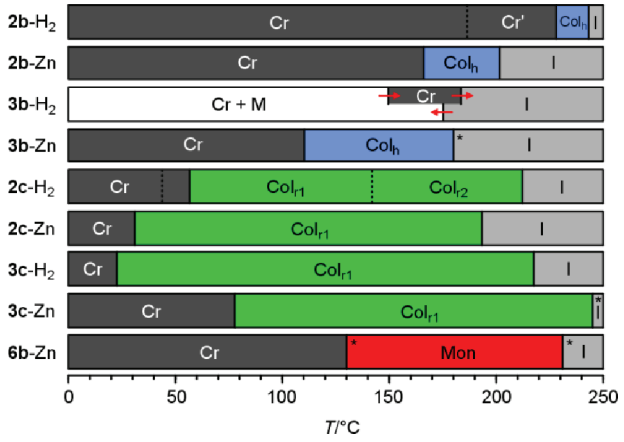

Figure 7. Thermal data for liquid-crystalline porphyrins, tetraphenanthroporphyrins, and tetra(benzochryseno)porphyrin obtained from differential scanning calorimetry. Symbols: Cr, crystalline or pseudocrystalline; Col, columnar phases; and I, isotropic liquid. *Transition detected by polarizing optical microscopy.

molecular volume V_M and columnar cross-section S (Table 3), is only slightly larger than h_{por}, indicating that the porphyrin rings are perpendicular to the columnar axis. Small off-axis tilts and lateral shifts of the macrocycles, resulting from thermal fluctuations, likely account for the small discrepancies between h_M and h_{por} values.

Zinc tetraphenanthroporphyrin **3b**-Zn forms a well-defined Col_h–*p6mm* phase between 110 and 180 °C, the identity of which was confirmed by XRD and DSC. The structural parameters of this phase (Table 2) closely resemble those determined for the corresponding porphyrin complex **2b**-Zn. This similarity is not surprising because molecular volumes of **2b**-Zn and **3b**-Zn are nearly identical, but it does not necessarily imply exact correspondence of the packing pattern. It should be noted that in **2b**-Zn, the core consists of a planar macrocycle surrounded by eight aryl groups, whereas in **3b**-Zn, the core comprises a single saddle-shaped π-system. In the latter case, the central part of the π system (porphyrin) and the peripheral "wings" (phenanthrene units) can still give rise to separate scattering signals (h_{por} and h_0, respectively). In contrast

dx.doi.org/10.1021/ja210991f | J. Am. Chem. Soc. 2012, 134, 4822–4833

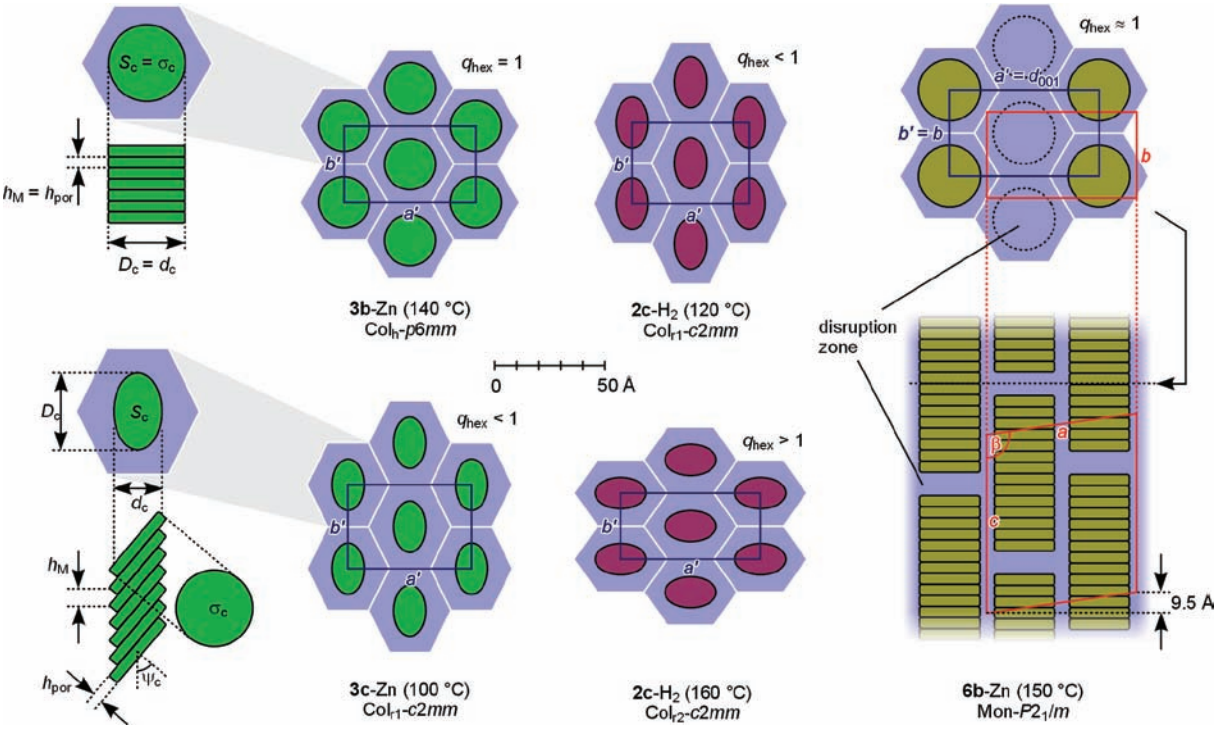

Figure 8. Packing diagrams for selected discotic mesophases. Effective core dimensions are indicated as colored ellipses. Alkyl chain continuum is shown in light blue, and a' and b' denote rectangular axes of the column packing sublattice; $q_{hex} = a'/(b'\sqrt{3})$. In the diagram of the Mon phase (right), the extent of the disruption zone along the c axis is arbitrary. Standard cell setting for the $P2_1/m$ space group is shown in red.

to porphyrins, these two signals are not well resolved in the wide-angle scattering pattern observed for **3b**-Zn.

In the Col$_h$ mesophase of **3b**-Zn, the stacking distance h_M = 5.0 Å is significantly smaller than the van der Waals thickness of the distorted tetraphenanthroporphyrin ring (ca. 8 Å, Figure 1). Consequently, the aromatic cores in the Col$_h$ phase must be packed quite tightly, with curvatures of adjacent π systems in the stack matched in a similar fashion as in the dimer [**3a**-Zn]$_2$. Thus the mean plane separations predicted for dimers [**3a**-H$_2$]$_2$ and [**3a**-Zn]$_2$ (z = 3.6–4.1 Å, Figure 3) constitute the lower limit of stacking height. In an actual stack the steric requirements imposed by neighboring molecules and peripheral substitution will likely be different than in the dimers, leading to an increase of the z distance. Curvature matching between consecutive molecules in the stack implies lateral displacements, analogous to that defined by the x vector in the [**3a**-Zn]$_2$ dimer. Experimental evidence for such displacements is provided by the effective core diameter D_c (23.2 Å), which is larger than the geometrical diameter of the tetraphenanthroporphyrin nucleus (19 Å, oxygen–oxygen distance in DFT models). An important observation, which follows from the earlier discussion of the dimer structure, is that consecutive x vectors within the stack cannot be collinear but have to be rotated by the angle φ (Figure 3) with respect to the column axis. Additionally, to make the stack grow along the column axis, the sense of rotation has to be the same for all x vectors, resulting in a helical arrangement of molecules. The φ angles are determined by the saddle-like shape of the π surface and should approximate the values obtained for the dimer models (Table 1). An idealized representation of the stacking paradigm outlined above can be obtained from molecular mechanics calculations. The helical stack shown in Figure 9 consists of 16 molecules of **3a**-Zn, yielding an average stacking distance of 4.5 Å. This value is smaller than the columnar slice thickness h_M, but it does not include the effect of thermal motions. In the actual Col$_h$ phase, the helical packing is likely effective only over short distances, combining sections of opposite helicity. The expected variability of the x, z, and φ parameters will contribute to the overall disorder within the stack.

Porphyrins **2c**-M and tetraphenanthroporphyrins **3c**-M (M = 2H, Zn), containing 16 dodecyl chains per molecule, form liquid crystalline phases at relatively low temperatures. These mesophases show excellent ranges of thermal stability and were fully characterized using XRD, DSC, and POM. For all systems of the **c** series, diffractograms showed a pair of fundamental reflections, (11) and (20), accompanied by several higher order peaks in the small-angle region. These features enabled unequivocal assignment of rectangular lattices with *c2mm* symmetry and determination of lattice parameters. In contrast to the **b** series, the reflections constituting the wide-angle diffuse signals are not as easily separable because of the much stronger contribution of the h_{ch} scattering (the volume fraction of the aliphatic continuum is doubled in the **c** series), and the smaller expected shift between h_{ch} and h_{por} at low temperature. For similar reasons, the h_0 peak cannot be precisely extracted. Porphyrin **2c**-H$_2$ exhibits a transition between two rectangular phases of *c2mm* symmetry, clearly evidenced by XRD and DSC data, that is not observed for other compounds in the **c** series. The two phases differ in the ordering of fundamental reflections: the low-temperature phase, denoted Col$_{r1}$, is characterized by $d_{11} > d_{20}$, similarly to other compounds in the **c** series. The order of reflections is inverted in the high-temperature phase Col$_{r2}$, which consequently has different lattice parameters. The q_{hex} ratio (Table 3, Figure 8), which expresses the distortion of the Col$_r$ lattices relative to the hexagonal lattice, takes values of ca. 0.8 for all Col$_{r1}$ phases, indicating that the lattice is compressed along the a direction (only the d_{20} fundamental periodicity is shrunken with respect

dx.doi.org/10.1021/ja210991f | J. Am. Chem. Soc. 2012, 134, 4822–4833

to the fundamental reflection of the Col_h phase of **2b**-H_2). For the unique Col_{r2} phase of **2c**-H_2, q_{hex} equals 1.2, corresponding to a compression of the lattice along the b direction (here, the reduced periodicity corresponds to two fundamental reflections d_{11} and $d_{1,-1}$).

The h_M values determined for the Col_{r1} and Col_{r2} phases are in the range of 7.1 to 8.3 Å, indicating that the macrocyclic cores must be tilted within the columns. The direction of the tilt coincides with the compressed axis in the rectangular lattice (Figure 8).[27] The Col_{r1} and Col_{r2} phases can be viewed as discotic analogs of smectic phases SmF and SmI, respectively. In the Col_{r1} and SmF phases, the molecules are tilted toward the edge of the pseudohexagonal network, whereas in the Col_{r2} and SmI phases the tilt is directed toward the nearest vertex of the lattice.[28] Geometrical parameters of the core in the Col_r phases, namely its effective cross-section σ_c, maximum and minimum diameter D_c and d_c and the tilt angle ψ_c can be calculated using data of the nontilted Col_h phases as a reference (Figure 8 and Table 3, see the Supporting Information for details of these calculations). A small divergence of the q_{hex} ratio (Table 2) with respect to the core ellipticity (d_c/D_c ratio) can be noticed for the investigated Col_r phases. This effect evidences the blurring out of the elliptical shape by the aliphatic continuum, possibly resulting from limited tilt correlation within the lattice plane.

As in the case of the Col_h phases, the curvatures of neighboring molecules in the stack will also have to be aligned in the tilted rectangular phases. The simplest arrangement of x vectors giving rise to a tilted stack is a zigzag pattern in which consecutive φ angles take opposite signs. Zigzag stacks of this kind constructed from the all-methoxy tetraphenanthroporphyrin molecules **3a**-H_2 yield a columnar slice thickness h_M of ca. 6 Å and a tilt angle ψ_c of approximately 45° (Figure 9). Both

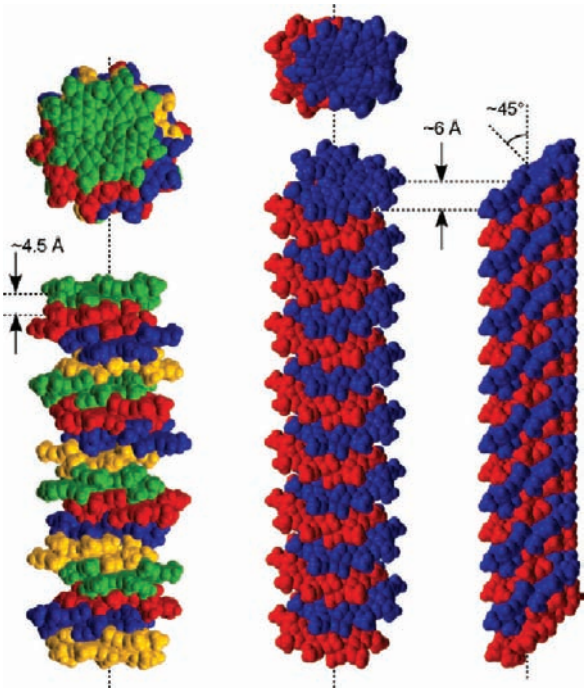

Figure 9. Models of helicoidal (left) and zigzag (right) columnar packing obtained for the all-methoxy tetraphenanthroporphyrin **3a**-H_2 (MM+).

parameters are underestimated relative to experimental data, indicating the influence of heavy peripheral substitution in the **c** series on the packing geometry within the columns.

In contrast to porphyrins and tetraphenanthroporphyrins described above, which display columnar phases with 2D ordering, zinc tetra(benzochryseno)porphyrin **6b**-Zn forms an unusual three-dimensional (3D) phase, denoted Mon, which is stable from ca. 130 to 232 °C. Formation of three-dimensionally ordered phases from discoid molecules is a rare phenomenon, typically involving bicontinuous phases with cubic symmetry.[29] XRD patterns recorded on cooling at three different temperatures contain up to 10 sharp, small-angle reflections, whose indexation converges toward a monoclinic lattice (Figure S20 and Tables S3 and S5, Supporting Information).[30] Given the presence of the (100) and (201) reflections, five space groups are compatible with the proposed indexation: groups $P2$, Pm, and $P2/m$ with no reflection conditions and the groups $P2_1$ and $P2_1/m$, where the occurrence of a 2_1 screw axis parallel to the b direction sets the condition $k = 2n$ for the $(0k0)$ reflections.[30] The absence of the (010) reflection makes the groups with screw axis more likely. Unit cell parameters determined at 100 °C yield a cell volume of 2.13×10^5 Å^3, corresponding to approximately 28 molecules of **6b**-Zn per unit cell.

The proposed organization of the Mon phase, shown in Figure 8, is analogous to a structure described recently in a series of semifluorinated dendrimers.[31] The mesophases formed by this family of dendrimers contained columns of segregating dendritic moieties and an aliphatic periphery. However, for the highest generation dendrimer, the columns disrupted into strings of elongated micelles. The relative positions of disruption zones in neighboring strings generated the $P2_1/m$ space group symmetry. In the Mon phase of **6b**-Zn, the 3D organization is generated with segments of rigid columns, instead of micelles, which lie along the c axis of the monoclinic lattice and are separated by disruption zones. As the $P2_1/m$ unit cell contains two such segments, each of them will contain an average of 14 discoid molecules, corresponding to a slice thickness h_M of ca. 5.7 Å, which is not much larger that the h_M values determined for the Col_h phases. The actual mean separation between discogens will be even smaller in the Mon phase, because the calculated h_M does not take into account the height of the disruption zone (the lower stacking limit, estimated for **6a**-H_2 using molecular modeling is ca. 4.8 Å). The small h_M value additionally indicates that the discogens should not show any systematic tilting within the column segment. In contrast to micelles, which are easily deformable, the envelope of the columnar segments cannot so easily deviate from cylindrical shape. The rigidity of these segments might explain the persistence of the near-perfect hexagonal symmetry of the columnar lattice ($q_{hex} \approx 1$), which is perpendicular to the c axis of the monoclinic cell (Figure 8). With respect to this sublattice plane (identifiable as d_{001}), the $[ab]$ plane is tilted by an angle of 8° (i.e., $\beta - \pi/2$), which corresponds to a vertical shift of the second neighboring row of columns of about 10 Å along the c direction ($a \times \sin(\beta - \pi/2) = 9.5$ Å). This shift is relatively small compared to the cell dimensions, making the resulting organization quite similar to either an orthorhombic or a 3D hexagonal lattice, in which consecutive rows of column sections are shifted by half the periodicity along the c direction. The symmetry breaking toward a monoclinic symmetry, observed for **6b**-Zn, is indicative of a subtle divergence of columns from the perfect cylindrical shape. In the absence of

dx.doi.org/10.1021/ja210991f | J. Am. Chem. Soc. 2012, 134, 4822−4833

tilting, this divergence has to be explained by other structural features, such as correlated off-axis shifts or dissymmetric ends of column segments.

The evolution of mesomorphism in the family of compounds described above can be explained by comparing the interface area between the discoid core and the aliphatic continuum with the requirements imposed by the pattern of peripheral substitution.[32] Interface areas Σ_c (Table 3) depend on the dimensions of the core and on column packing and were calculated using reported dilatometric data.[25] On the basis of the interface area, the chain packing ratio can be defined as $q_{ch} = (\Sigma_c/N_c)/\sigma_{ch}$, where N_c is the number of peripheral functional groups (16 for porphyrins and tetraphenanthroporphyrins, 24 for tetra(benzochryseno)porphyrin) and σ_{ch} is the effective cross-section of a stretched alkyl chain at the temperature of measurement. In the **c** series, q_{ch} is approximately 1.3, indicating that the 16 dodecyl chains would exceed the available interface area in the case of an untilted arrangement and that the area matching is achieved by tilting the cores relative to the column axis. For Col_h phases of the **b** series, the presence of smaller methyl substituents enables other mechanisms of area matching, such as expulsion of substitutents from the interface by fluctuations in the columnar stacking. In the case of **6b**-Zn neither of the above mechanisms is apparently sufficient to overcome steric crowding of alkyl chains at the interface, because of the packing requirements of 24 peripheral groups attached to the macrocycle exceed the available interface area ($q_{ch} \approx 0.84$ for a theoretical tilted arrangement). The surface area is however expanded by folding some of the chains over the ends of the columnar segments (Figure 8), leading to the formation of disruption zones between them. This mechanism of surface matching is potentially more efficient than it could be for porphyrins and tetraphenanthroporphyrins because of the larger effective cross-section of the macrocyclic core of **6b**-Zn.

CONCLUSIONS

The strategy of expanding the porphyrin π system via fusion of adjacent β-substituents, which is presented in this paper, provides access to new condensed systems, whose physical properties have been studied in detail. Facile peripheral functionalization of tetraphenanthroporphyrins not only overcomes solubility problems encountered in earlier work but also gives access to derivatives displaying thermotropic liquid crystallinity. The successful synthesis of tetra(benzochryseno)porphyrin shows that the present method provides access to highly congested π-electron systems that might be difficult to synthesize directly from sterically hindered monopyrroles. In comparison with tetraphenanthroporphyrins, this new macrocyclic system exhibits a significant enhancement of Q-band intensity. This feature suggests that molar absorptivities may be further increased in larger systems based on the present structural paradigm. Our synthetic strategy, which relies on the use of the Scholl reaction, may be sufficiently general to provide access to such systems.

Self-assembly of phenanthroporphyrins into columnar mesophases, investigated for several mesomorphic derivatives, is shown to depend on the inherent curvature of the π-conjugated cores and on peripheral substitution. Using simple geometrical arguments, supported by computational data, we were able show a relationship between the dimerization of tetraphenanthroporphyrins observed in solution and the stacking patterns available for the columnar structures. Formation of the unique 3D mesophase of tetra(benzochryseno)porphyrin shows that peripherally fused porphyrin derivatives provide a potentially general class of core motifs for construction of structurally nontrivial liquid-crystalline materials. Further extension of this work may help in tailoring mesophase structures of large nonplanar aromatics so as to meet specific needs of molecular electronics applications.

ASSOCIATED CONTENT

Supporting Information

Synthetic procedures, analytical data, and computational details. This material is available free of charge via the Internet at http://pubs.acs.org.

AUTHOR INFORMATION

Corresponding Author

marcin.stepien@chem.uni.wroc.pl

ACKNOWLEDGMENTS

Financial support from the Ministry of Science and Higher Education (decision 105/10/E-344/M/2011) is gratefully acknowledged. We thank the Foundation for Polish Science for financial support at an early stage of this project. Quantum chemical calculations were performed in the Wrocław Center for Networking and Supercomputing. We thank Piotr Stefanowicz for recording mass spectra. B.D. and B.H. thank the CNRS and University Strasbourg for support and D. Burger for the TGA measurements (IPCMS, le service commun d'analyse de l'Université de Strasbourg).

REFERENCES

(1) (a) Wu, J.; Pisula, W.; Müllen, K. *Chem. Rev.* **2007**, *107*, 718–747. (b) Chou, J.-H.; Nalwa, H. S.; Kosal, M. E.; Rakow, N. A.; Suslick, K. S. Applications of Porphyrins and Metalloporphyrins to Materials Chemistry. In *The Porphyrin Handbook*; Kadish, K. M., Smith, K. M., Guilard, R., Eds.; Academic Press: San Diego, CA, 2000; Vol. *6* p 43. (c) Fukuzumi, S. Artificial Photosynthetic Systems Composed of Porphyrins and Phthalocyanines. In *Handbook of Porphyrin Science*; Kadish, K. M., Smith, K. M., Guilard, R., Eds.; World Scientific Publishing: Hackensack, NJ, 2010; Vol. *5* p 183. (d) Dini, D.; Hanack, M. Physical Properties of Phthalocyanine-based Materials. In *The Porphyrin Handbook*; Kadish, K. M., Smith, K. M., Guilard, R., Eds.; Academic Press: San Diego, CA, 2003; Vol. *17* pp 1–36.

(2) (a) Murphy, A. R.; Fréchet, J. M. J. *Chem. Rev.* **2007**, *107*, 1066–1096. (b) Coropceanu, V.; Jérôme, C.; da Silva Filho, D. A.; Olivier, Y.; Silbey, R.; Brédas, J.-L. *Chem. Rev.* **2007**, *107*, 926–952. (c) Pron, A.; Gawrys, P.; Zagorska, M.; Djurado, D.; Demadrille, R. *Chem. Soc. Rev.* **2010**, *39*, 2577–2632. (d) Warman, J. M.; van de Craats, A. M. *Mol. Cryst. Liq. Cryst.* **2003**, *396*, 41. (e) Hains, A. W.; Liang, Z.; Woodhouse, M. A.; Gregg, B. A. *Chem. Rev.* **2010**, *110*, 6689–6735.

(3) (a) Rosen, B. M.; Wilson, C. J.; Wilson, D. A.; Peterca, M.; Imam, M. R.; Percec, V. *Chem. Rev.* **2009**, *109*, 6275–6540. (b) Donnio, B.; Guillon, D.; Deschenaux, R.; Bruce, D. W. Metallomesogens. In *Comprehensive Coordination Chemistry II*; Elsevier: Waltham, MA, 2003; Vol. *7*, pp 357–627.

(4) (a) Stępień, M.; Sprutta, N.; Latos-Grażyński, L. *Angew. Chem., Int. Ed.* **2011**, *50*, 4288–4340. (b) Saito, S.; Osuka, A. *Angew. Chem., Int. Ed.* **2011**, *50*, 4342–4373. (c) Sessler, J. L.; Seidel, D. *Angew. Chem., Int. Ed.* **2003**, *42*, 5134–5175.

(5) (a) Kim, D.; Osuka, A. *Acc. Chem. Res.* **2004**, *37*, 735–745. (b) Aratani, N.; Kim, D.; Osuka, A. *Acc. Chem. Res.* **2009**, *42*, 1922–1934. Recent examples: dimeric (c) Sakurai, T.; Shi, K.; Sato, H.; Tashiro, K.; Osuka, A.; Saeki, A.; Seki, S.; Tagawa, S.; Sasaki, S.; Masunaga, H.; Osaka, K.; Takata, M.; Aida, T. *J. Am. Chem. Soc.* **2008**, *130*, 13812–13813. (d) Sakurai, T.; Tashiro, K.; Honsho, Y.; Saeki, A.;

Seki, S.; Osuka, A.; Muranaka, A.; Uchiyama, M.; Kim, J.; Ha, S.; Kato, K.; Takata, M.; Aida, T. *J. Am. Chem. Soc.* **2011**, *133*, 6537−6540. Square: (e) Nakamura, N.; Aratani, N.; Shinokubo, H.; Takagi, A.; Kawai, T.; Matsumoto, T.; Yoon, Z. S.; Kim, D. Y.; Ahn, T. K.; Kim, D.; Muranaka, A.; Kobayashi, N.; Osuka, A. *J. Am. Chem. Soc.* **2006**, *128*, 4119−4127. Nanorings: (f) Hoffmann, M.; Wilson, C. J.; Odell, B.; Anderson, H. L. *Angew. Chem., Int. Ed.* **2007**, *46*, 3122−3125. (g) O'Sullivan, M. C.; Sprafke, J. K.; Kondratuk, D. V.; Rinfray, C.; Claridge, T. D. W.; Saywell, A.; Blunt, M. O.; O'Shea, J. N.; Beton, P. H.; Malfois, M.; Anderson, H. L. *Nature* **2011**, *469*, 72−75.

(6) General reviews: (a) Ono, N.; Yamada, H.; Okujima, T. Synthesis of Porphyrins Fused with Aromatic Rings. In *Handbook of Porphyrin Science*; Kadish, K. M., Smith, K. M., Guilard, R., Eds.; World Scientific Publishing: Hackensack, NJ, 2010; Vol. *2* p 1. (b) Lash, T. D. Syntheses of Novel Porphyrinoid Chromophores. In *The Porphyrin Handbook*; Kadish, K. M.; Smith, K. M.; Guilard, R.; Academic Press: San Diego, CA, 2000; Vol. *2* p 125.

(7) Meso-*β*-fused arenes. Naphthalene: (a) Gill, H. S.; Harmjanz, M.; Santamara, J.; Finger, I.; Scott, M. J. *Angew. Chem., Int. Ed.* **2004**, *43*, 485−490. (b) Hayashi, S.; Tanaka, M.; Hayashi, H.; Eu, S.; Umeyama, T.; Matano, Y.; Araki, Y.; Imahori, H. *J. Phys. Chem. C* **2008**, *112*, 15576−15585. Azulene: (c) Kurotobi, K.; Kim, K. S.; Noh, S. B.; Kim, D.; Osuka, A. *Angew. Chem., Int. Ed.* **2006**, *45*, 3944−3947. Anthracene: (d) Davis, N. K. S.; Pawlicki, M.; Anderson, H. L. *Org. Lett.* **2008**, *10*, 3945−3947. (e) Davis, N. K. S.; Thompson, A. L.; Anderson, H. L. *Org. Lett.* **2010**, *12*, 2124−2127. (f) Davis, N. K. S.; Thompson, A. L.; Anderson, H. L. *J. Am. Chem. Soc.* **2011**, *133*, 30−31. Pyrene: (g) Yamane, O.; Sugiura, K.; Miyasaka, H.; Nakamura, K.; Fujimoto, T.; Nakamura, K.; Kaneda, T.; Sakata, Y.; Yamashita, M. *Chem. Lett.* **2004**, *33*, 40−41. (h) Diev, V. V.; Hanson, K.; Zimmerman, J. D.; Forrest, S. R.; Thompson, M. E. *Angew. Chem., Int. Ed.* **2010**, *49*, 5523−5526. Perylene: (i) Jiao, C. J.; Huang, K. W.; Guan, Z. P.; Xu, Q. H.; Wu, J. S. *Org. Lett.* **2010**, *12*, 4046−4049.

(8) *β*-*β*-Fused arenes. Benzene: (a) Finikova, O. S.; Cheprakov, A.; Beletskaya, I.; Vinogradov, S. *Chem. Commun.* **2001**, 261. (b) Finikova, O. S.; Cheprakov, A.; Beletskaya, I. P.; Carroll, P. J.; Vinogradov, S. A. *J. Org. Chem.* **2004**, *69*, 522 and references therein. Naphthalene: (c) Finikova, O.; Cheprakov, V.; Vinogradov, S. *J. Org. Chem.* **2005**, *70*, 9562−9572. Anthracene: (d) Yakutkin, V.; Alekshchenkov, S.; Chernov, S; Miteva, T.; Nelles, G.; Cheprakov, A.; Baluschev, S. *Chem.—Eur. J.* **2008**, *14*, 9846. Phenanthrene: (e) Lash, T. D; Novak, B. H. *Angew. Chem., Int. Ed. Engl.* **1995**, *34*, 638. (f) Ono, N.; Hironaga, H.; Ono, K.; Kaneko, S.; Murashima, T.; Ueda, T.; Tsukamura, C.; Ogawa, T. *J. Chem. Soc., Perkin Trans. 1.* **1996**, 41. (g) Novak, B. H.; Lash, T. D. *J. Org. Chem.* **1998**, *63*, 3998. (h) Xu, H.-J.; Shen, Z.; Okujima, T.; Ono, N.; You, X.-Z. *Tetrahedron Lett.* **2006**, *47*, 931−934. (i) Xu, H.-J.; Mack, J.; Descalzo, A. B.; Shen, Z.; Kobayashi, N.; You, X.-Z.; Rurack, K. *Chem.—Eur. J.* **2011**, *17*, 8965−8983. Fluoranthrene: (j) Lash, T. D.; Werner, T. M.; Thompson, M. L.; Manley, J. M. *J. Org. Chem.* **2001**, *66*, 3152−3159. Corannulene: (k) Boedigheimer, H.; Ferrence, G. M.; Lash, T. D. *J. Org. Chem.* **2010**, *75*, 2518. Triphenylene: (l) Jiang, L.; Engle, J. T.; Sirk, L.; Hartley, C. S.; Ziegler, C. J.; Wang, H. *Org. Lett.* **2011**, *13*, 3020.

(9) For alternative approaches to elaboration of *β*-*β* fused rings see ref 8l. Peripherally fused phthalocyanie derivatives: (a) Cammidge, A. N.; Gopee, H. *Chem. Commun.* **2002**, 966−967. (b) Cammidge, A. N.; Gopee, H. *Chem.—Eur. J.* **2006**, *12*, 8609−8613. (c) Cammidge, A. N.; Gopee, H. *J. Porphyrins Phthalocyanines* **2009**, *13*, 235−246.

(10) LC porphyrinoids: (a) Sessler, J. L.; Callaway, W. B.; Dudek, S. P.; Date, R. W.; Lynch, V.; Bruce, D. W. *Chem. Commun.* **2003**, 2422−2423. (b) Sessler, J. L.; Callaway, W. B.; Dudek, S. P.; Date, R. W.; Bruce, D. W. *Inorg. Chem.* **2004**, *43*, 6650−6653. (c) Stępień, M.; Donnio, B.; Sessler, J. L. *Angew. Chem., Int. Ed.* **2007**, *46*, 1431−1435. (d) Stępień, M.; Donnio, B.; Sessler, J. L. *Chem.—Eur. J.* **2007**, *13*, 6853−6863 ; see also refs 5c and 5d and 9a−9c.

(11) (a) Lindsey, J. S.; Schreiman, I. C.; Hsu, H. C.; Kearney, P. C.; Marguerettaz, A. M. *J. Org. Chem.* **1987**, *52*, 827−836. (b) Lindsey, J. S. Synthesis of meso-Substituted Porphyrins. In *The Porphyrin Handbook*; Kadish, K. M., Smith, K. M., Guilard, R., Eds.; Academic Press: San Diego, CA, 2000; Vol. *1*, pp 45−118.

(12) Barton, D. H. R.; Kervagoret, J.; Zard, S. Z. *Tetrahedron* **1990**, *46*, 7587−7598. Bullington, J. L.; Wolff, R. R.; Jackson, P. F. *J. Org. Chem.* **2002**, *67*, 9439.

(13) See for instance: (a) King, B. T.; Kroulík, J.; Robertson, C. R.; Rempala, P.; Hilton, C. L.; Korinek, J. D.; Gortari, L. M. *J. Org. Chem.* **2007**, *72*, 2279−2288. (b) Ormsby, J. L.; Black, T. D.; Hilton, C. L.; Bharat; King, B. T. *Tetrahedron* **2008**, *64*, 11370−11378. (c) Wadumethrige, S. H.; Rathore, R. *Org. Lett.* **2008**, *10*, 5139−5142.

(14) For general references on porphyrin aggregation and their spectroscopic efects see: (a) Hunter, C. A.; Sanders, J. K. M. *J. Am. Chem. Soc.* **1990**, *112*, 5525−5534. (b) Hunter., C. A.; Lawson, K. R.; Perkins, J.; Urch, C. J. *J. Chem. Soc., Perkin Trans. 2* **2001**, 651−669. (c) Medforth, C. J. NMR Spectroscopy of Diamagnetic Porphyrins. In *The Porphyrin Handbook*; Academic Press: San Diego, CA, 2000; Vol. *5*, pp 1−80. (d) Snow, A. W. Phthalocyanine Aggregation. In *The Porphyrin Handbook*; Academic Press: San Diego, CA, 2003; Vol. *17*, pp 129−176.

(15) (a) The *ω*B97XD functional: Chai, J.-D.; Head-Gordon, M. *Phys. Chem. Chem. Phys.* **2008**, *10*, 6615−6620. (b) Performance of MM methods in the modeling of *π*-aromatic interactions: Paton, R. S.; Goodman, J. M. *J. Chem. Inf. Model.* **2009**, *49*, 944−955. Porphine dimerization is an interesting reference case; see (c) Mück-lichtenfeld, C.; Grimme, S. *Mol. Phys.* **2007**, *105*, 2793−2798; DOI: 10.1080/00268970701635543 and references therein.

(16) (a) Littler, B. J.; Ciringh, Y.; Lindsey, J. S. *J. Org. Chem.* **1999**, *64*, 2864. (b) Geier, G. R.; Callinan, J. B.; Rao, P. D.; Lindsey, J. S. *J. Porphyrins Phthalocyanines* **2001**, *5*, 810.

(17) The trivial name tetra(benzochryseno)porphyrin, chosen here for simplicity, does not correspond to the IUPAC-recommended selection of attached components. The IUPAC name for the ring system of **6**-H_2 is tetrabenzo[3,4:3′,4′:3″,4″:3‴,4‴]tetrakistriphenyleno[1,2-*b*:1′,2′-*g*:1″,2″-*l*:1‴,2‴-*q*]porphyrin; see Moss, G. P. *Pure Appl. Chem.* **1998**, *70*, 143−216.

(18) A similar twist was observed in the solid-state structure of octamethoxydibenzochrysene: Navale, T. S.; Zhai, L; Lindeman, S. V.; Rathore, R. *Chem. Commun.* **2009**, 2857−2859.

(19) Zhang, G.; Musgrave, C. B. *J. Phys. Chem. A* **2007**, *111*, 1554−1561.

(20) Kobayashi, N. Synthesis and Properties of Phthalocyanine Analogs. In *The Porphyrin Handbook*; Kadish, K. M., Smith, K. M., Guilard, R., Eds.; Academic Press: San Diego, CA, 2003; Vol. *15* pp 161−262. For a compilation of relevant data for peripherally fused porphyrinoids, see ref 6b.

(21) Seidel, D.; Lynch, V.; Sessler, J. L. *Angew. Chem., Int. Ed.* **2002**, *41*, 1422−1425.

(22) Gouterman, M. In *The Porphyrins*; Dolphin, D., Ed.; Academic: New York, 1978; Vol. *III*, Part A, Physical Chemistry.

(23) For detailed XRD, DSC, and POM data see Tables and Figures in the Supporting Information.

(24) Compound **3b**-H_2 forms a slowly crystallizing monotropic mesophase, which could not be reliably analyzed by XRD or POM.

(25) The temperature dependence of h_{ch} is in full agreement with the relationship deduced from previously published temperature expansion experiments: $h_{ch} = 0.9763 \times \sqrt{\sigma_{ch}}$, with $\sigma_{ch} = V_{CH2}/1.27$. See: Marcos, M.; Giménez, R.; Serrano, J. L.; Donnio, B.; Heinrich, B.; Guillon, D. *Chem.—Eur. J.* **2001**, *7*, 1006.

(26) For instance, in the X-ray structure of 2,3,5,10,12,13,15,20-octaphenylporphyrin (mixed meso- and *β*-substitution), the stacking distance is 4.56 Å. Chan, K. S.; Zhou, X.; Luo, B.-s.; Mak, T. C. W. *Chem. Commun.* **1994**, 271.

(27) Morale, F.; Date, R. W.; Guillon, D.; Bruce, D. W.; Finn, R. L.; Wilson, C.; Blake, A. J.; Schröder, M.; Donnio, B. *Chem.—Eur. J.* **2003**, *9*, 2484−2501. Donnio, B.; Heinrich, B.; Allouchi, H.; Kain, J.; Diele, S.; Guillon, D.; Bruce, D. W. *J. Am. Chem. Soc.* **2004**, *126*, 15258−15268.

(28) Gray, G. W.; Goodby, J. W. *Smectic Liquid Crystals; Textures and Structures*; Leonard Hill: Glasgow, Scotland, 1984.

(29) (a) Hatsusaka, K.; Ohta, K.; Yamamoto, I.; Shirai, H. *J. Mater. Chem.* **2001**, *11*, 423−433. (b) Ichihara, M.; Suzuki, A.; Hatsusaka, K.; Ohta, K. *Liq. Cryst.* **2007**, *34*, 555−567. (c) Alam, M. A.; Motoyanagi, J.; Yamamoto, Y.; Fukushima, T.; Kim, J.; Kato, K.; Takata, M.; Saeki, A.; Seki, S.; Tagawa, S.; Aida, T. *J. Am. Chem. Soc.* **2009**, *131*, 17722−17723.

(30) *International Tables for Crystallography, Vol. A*, 4th ed.; Hahn, T., Ed.; The International Union of Crystallography; Kluwer Academic: Dordrecht, The Netherlands, 1995.

(31) Bury, I.; Heinrich, B.; Bourgogne, C.; Mehl, G. H.; Guillon, D.; Donnnio, B. *New. J. Chem.* **2012**, advance article, DOI 10.1039/c1nj20530g.

(32) Donnio, B.; Heinrich, B.; Gulik-Grzywicki, T.; Delacroix, H.; Guillon, D. *Chem. Mater.* **1997**, *12*, 2951−2965.